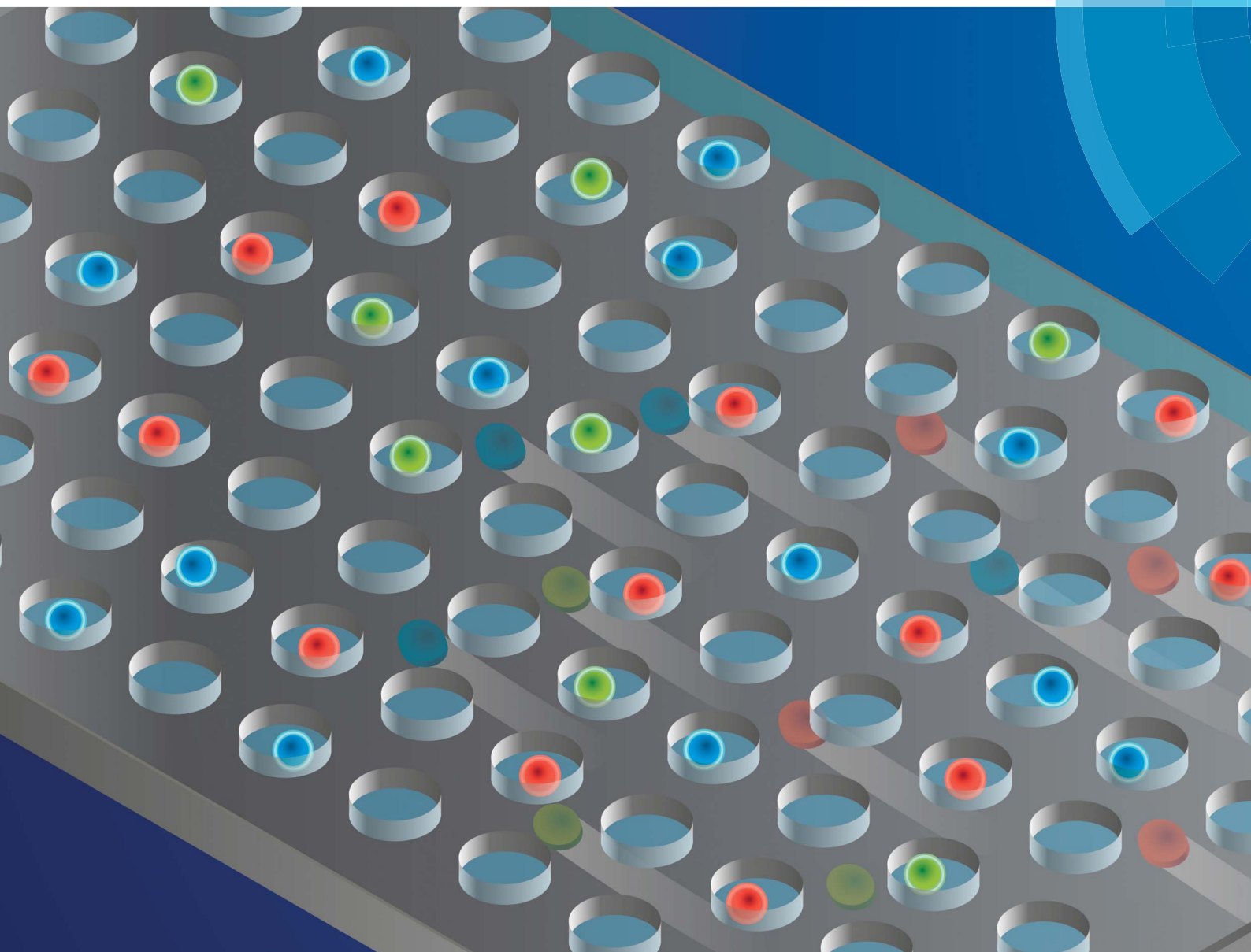


Soft Matter

www.softmatter.org



ISSN 1744-683X



PAPER

Patricia Bassereau, Charles N. Baroud *et al.*

Trapping and release of giant unilamellar vesicles in microfluidic wells

PAPER

Cite this: *Soft Matter*, 2014, 10, 5878

Trapping and release of giant unilamellar vesicles in microfluidic wells†

Ayako Yamada,^a Sungyon Lee,^b Patricia Bassereau*^a and Charles N. Baroud*^c

We describe the trapping and release of giant unilamellar vesicles (GUVs) in a thin and wide microfluidic channel, as they cross indentations etched in the channel ceiling. This trapping results from the reduction of the membrane elastic energy, which is stored in the GUV as it squeezes to enter into the thin channel. We demonstrate that GUVs whose diameter is slightly larger than the channel height can be trapped and that they can be untrapped by flowing the outer fluid beyond a critical velocity. GUVs smaller than the channel height flow undisturbed while those much larger cannot squeeze into the thin regions. Within the range that allows trapping, larger GUVs are anchored more strongly than smaller GUVs. The ability to trap vesicles provides optical access to the GUVs for extended periods of time; this allows the observation of recirculation flows on the surface of the GUVs, in the forward direction near the mid-plane of the channel and in the reverse direction elsewhere. We also obtain the shape of GUVs under different flow conditions through confocal microscopy. This geometric information is used to derive a mechanical model of the force balance that equates the viscous effects from the outer flow with the elastic effects based on the variation of the membrane stretching energy. This model yields good agreement with the experimental data when values of the stretching moduli are taken from the scientific literature. This microfluidic approach provides a new way of storing a large number of GUVs at specific locations, with or without the presence of an outer flow. As such, it constitutes a high-throughput alternative to micropipette manipulation of individual GUVs for chemical or biological applications.

Received 10th January 2014
Accepted 30th April 2014

DOI: 10.1039/c4sm00065j

www.rsc.org/softmatter

Introduction

Cells are subjected to many changes in shape and in size during their life cycle. This observation had motivated the early development of continuum models and mechanical experiments on lipid model membrane systems.^{1–4} Because they have sizes similar to cells, Giant Unilamellar Vesicles (GUVs) are very convenient model membrane systems and have been used to investigate various cellular phenomena in reconstituted systems, allowing direct observation by optical microscopy.^{5,6} Indeed, GUVs consist of an assembly of phospholipids that form a closed bilayer membrane (also called liposome) in an aqueous environment with diameters ranging from a few microns to tens of microns. Mechanical properties of lipid membranes can be measured precisely, using, for instance,

micropipette aspiration^{4,7,8} or analysing their thermal fluctuations.^{9,10} These experiments are generally technically delicate and performed on a single GUV at a time, making it tedious to obtain reasonable statistics. Although GUVs are known to be fragile, *i.e.* lipid membranes are hardly stretchable and easily rupture under tension, one of the challenges in membrane characterization is to manipulate GUVs in a controlled high-throughput manner.

In this context, microfluidic technologies constitute a promising path to explore. Indeed, recent developments in microfluidics have enabled the handling of micron-sized objects, such as cells, droplets, and particles in large quantities under a controlled environment.^{11–15} It has also been successfully applied to study the behaviour of micron-sized deformable objects, *e.g.* GUVs,^{16,17} cells,^{18–20} capsules,^{21,22} and water-in-oil (w/o) droplets²³ flowing in confined geometries. However it has generally remained difficult to keep these objects stationary in order to obtain long-term observations.

In contrast with classical microfluidic systems, where objects constantly flow in a narrow channel, a few groups^{24–28} have recently developed microfluidic methods to anchor liquid droplets or gas bubbles. In particular, Baroud *et al.*,^{26–28} etched small wells on the top surface of a channel in a Hele-Shaw configuration. When a droplet or an air bubble is squeezed in a

^aInstitut Curie, Centre de Recherche; CNRS, UMR168; Université Pierre et Marie Curie; Labex CelTisPhyBio and Paris Sciences et Lettres, F-75248 Paris Cedex 05, France. E-mail: patricia.bassereau@curie.fr

^bDepartment of Mechanical Engineering, Texas A&M, College Station, TX 77843, USA

^cLaboratoire d'Hydrodynamique (LabHyX) and Department of Mechanics, Ecole Polytechnique, CNRS, 91128 Palaiseau, France. E-mail: baroud@ladhyx.polytechnique.fr

† Electronic supplementary information (ESI) available: Movies S1–S3, Fig. S1 and S2, and description of movies. See DOI: 10.1039/c4sm00065j

channel with a height smaller than its diameter, it carries excess surface energy due to the deformation caused by the confinement. When coming across a well with a larger height, the droplet/bubble can slightly relax its area, and then gets trapped by the attractive force produced by the surface energy gradient. The trapping efficiency is strong enough to anchor a droplet or a bubble against an outer flow but increasing the flow velocity above a threshold value will release the drop from the anchor.

While such a trapping mechanism would be useful for high-throughput studies of GUVs, it is not clear *a priori* if a similar anchoring mechanism would apply. Indeed, GUVs can only increase their surface area by a few percent before rupturing, contrary to drops and bubbles that do not have such limits. It is therefore not clear that the variation in free energy of a vesicle is sufficient to counteract the drag force due to the external flow.

Below we report the ability to trap GUVs in an analogous microfluidic device but with wells larger than the diameter of the GUVs. We determine the range of flow rates at which GUVs are trapped, and we describe the vesicle shape and flow on its surface at a moderate flow rate. Finally, we investigate the release of GUVs at critical flow velocities depending on lipid compositions and compare the results to the elastic membrane model based on published membrane stretching moduli, K_A .

Materials and methods

Microfluidic device fabrication

The microfluidic device was fabricated in poly-dimethylsiloxane (PDMS) according to the design depicted in Fig. 1. The channel height and the well depth are $30\ \mu\text{m}$, the channel width is $3\ \text{mm}$, and the diameter of the wells is $110\ \mu\text{m}$. The master for the device was fabricated using the dry film photoresist soft lithography technique.²⁹ In this method, successive layers of a solid photoresist are deposited and exposed to UV using a succession of masks that determine the features at each height.

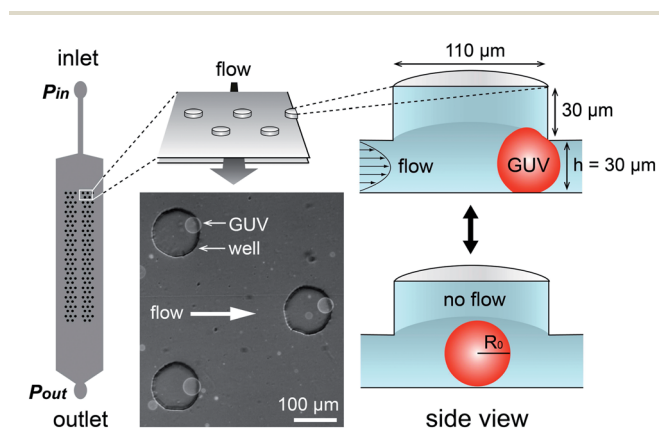


Fig. 1 Scheme of the microfluidic device for trapping giant unilamellar vesicles (GUVs): top view of the whole channel (left), close-up view of wells etched into the ceiling of the channel (upper middle), and side view of a well with a trapped GUV (right). Fluorescence microscopy image of trapped GUVs containing a fluorescent lipid and phase contrast image of wells etched on the top surface of the microfluidic channel taken from the bottom of the channel (lower middle).

Once all layers are deposited and exposed, the complete device is developed to reveal the mold that is then used to produce the PDMS devices. This procedure is rapid (few minutes) and simple to implement; it does not require a mask aligner since it relies on superposing millimeter-scale structures.

PDMS and its linker of the Sylgard 184 kit (Dow Corning) were mixed at the ratio of $10 : 1$ (w/w), poured on the master, and degassed. After more than 4 h of incubation at $60\ ^\circ\text{C}$, the PDMS chip was cut and removed from the master.

GUV preparation

Non-fluorescent lipids, *L*- α -phosphatidylcholine from chicken egg (EPC), 1,2-dioleoyl-*sn*-glycero-3-phosphocholine (DOPC), cholesterol (chol), and sphingomyelin from porcine brain (SM) were purchased from Avanti Polar Lipids. A fluorescent lipid, Texas Red 1,2-dihexadecanoyl-*sn*-glycero-3-phosphoethanolamine (Texas Red DHPE), was obtained from Life Technologies. GUVs were prepared by an electro-formation method as follows.³⁰ Lipids including 0.5% (w/w) Texas Red DHPE were dissolved and mixed well in chloroform at the total lipid concentration of $0.5\ \text{mg}\ \text{ml}^{-1}$. The lipid mixture was spread onto the conductive surfaces of two indium tin oxide-coated glass slides (ITO slides, Präzisions Glas & Optik), which were warmed up at $50\ ^\circ\text{C}$ prior to the lipid deposition by using a glass syringe (Hamilton). The obtained lipid films on ITO slides were further dried under vacuum for 2 h at room temperature. Milli-Q water or 3 mM sucrose solution was then sealed between the lipid-deposited surfaces of ITO slides by using sigillum wax (Vitrex Medical A/S). Immediately after sealing, 1 V AC voltage at 10 Hz was applied between the ITO slides under light shielding to grow GUVs, for 4 h at $50\ ^\circ\text{C}$ for the mixture of SM and chol, and at room temperature for the other compositions. The GUV solution was collected in a microcentrifuge tube, kept at $4\ ^\circ\text{C}$, and used within 2 days.

GUVs electro-formed in 3 mM sucrose solution were used as 'pre-stretched' GUVs after 10–20 times dilution in Milli-Q water whereas 'non-pre-stretched' GUVs were electro-formed in Milli-Q water. Pre-stretching allows the removal of membrane defects due to GUV preparation and is normally required to measure membrane stretching properties, *e.g.* by the micropipette aspiration technique.³¹

GUV trapping experiments

A PDMS chip with punched inlet and outlet holes was placed under vacuum for 3 min prior to bonding with a glass microscope slide using oxygen plasma. Immediately after bonding, $0.5\ \text{mg}\ \text{ml}^{-1}$ β -casein in phosphate buffered saline (Sigma Aldrich) was introduced in the channel using a micro-pipette. Owing to the vacuum treatment, air bubbles trapped in wells during this process went out of the channel through the PDMS wall. The chip was incubated with the solution for 5 min at room temperature to deactivate the channel surface to avoid GUV adhesion. The GUV solution 10–20 times diluted with Milli-Q water was introduced into the channel using a pressure pump (MFCS-FLEX, Fluigent) under microscopy observation.

Note that β -casein solution was completely replaced by the GUV solution before measurements.

During the course of an experiment, the flow was controlled through a pressure difference between the inlet and the outlet of the channel. This pressure drop $\Delta P = P_{\text{in}} - P_{\text{out}}$ could be related to the velocity of the fluid U by modelling each section of the channel as a linear resistor and summing up the resistors in series. We obtained $U(\text{mm s}^{-1}) = 5 \times 10^{-2} \Delta P(\text{mbar})$ in the wide region of the microchannel. This relationship was validated experimentally by observing the flow of fluorescent particles as a function of the imposed pressure drop.

Once GUVs were trapped in wells, the pressure at the channel inlet was decreased to reach $\Delta P = 0$. Fluorescence and phase-contrast images of GUVs and wells in the channel at $\Delta P = 0$ were recorded with a CCD camera (CoolSnap ES, Photometrics) and MetaView software (Universal Imaging) through a $10\times$ objective on an inverted fluorescence microscope (Axiovert 135, Zeiss). ΔP was then gradually increased again until the GUVs escaped from the wells. The critical ΔP upon escape, ΔP_c , was recorded for each GUV. Lipid flow in a GUV membrane at a fixed ΔP was recorded in the same configuration. Stacks of confocal images of GUVs were taken to visualize the three dimensional deformation of GUVs through a $100\times$ or a $40\times$ oil immersion objective on a confocal microscope (Eclipse TE 2000-E with a D-Eclipse C1 confocal head, Nikon, or LSM 510 META, Zeiss). All the experiments were performed at room temperature. Image analysis was done using ImageJ software.

Experimental results

1. Vesicles in a range of sizes can be trapped

In this work, we used electroformation to produce giant vesicles since this method is recognized to produce more than 90% of unilamellar vesicles.³⁰ After electroformation the initial size distribution of GUVs covers a wide range, as shown by the size distribution in ESI Fig. S1.† When such a GUV solution is injected into the microchannel from the inlet, the vesicles have varying fates depending on their sizes. The small vesicles, whose diameter is smaller than the channel height ($30\ \mu\text{m}$), simply flow through and exit the channel. In contrast, vesicles much larger than the channel height are blocked at the inlet junction and sometimes explode due to shear, producing some “ghost” membranes that often adhere to the channel surface. Finally, GUVs with a diameter slightly larger than $30\ \mu\text{m}$ can be successfully trapped in the wells.

At high density of GUV, *i.e.* without dilution after electroformation, multiple GUVs were trapped in each well. By diluting the GUV solution 10–20 times depending on the GUV density, we could achieve the trapping of a few tens of isolated GUVs in wells as shown in the lower middle image of Fig. 1. All the measurements shown below were performed on the individualised GUVs.

The trapping efficiency was measured by obtaining the size distribution of GUVs that could be trapped in the device, as the lipid composition was varied, as shown in Fig. 2. We observe that the device selects vesicles in a narrow range of diameters, often in the $30\text{--}50\ \mu\text{m}$ range. This however is not true for the

$7:3$ EPC and cholesterol (mol/mol) vesicles without pre-stretching, for which we have observed larger vesicles entering the channel and getting trapped, suggesting a very high fraction of membrane defects in the GUVs with this composition. Nevertheless, when pre-stretched, the GUVs show a narrower distribution of sizes that could be trapped, similar for all lipid compositions (filled bars).

2. Flow on a trapped vesicle

Although the vesicle itself is stationary in the well when trapped, the moving outer fluid causes a flow on the interface. This flow was visualized by tracking some fluorescent lipid inhomogeneities in the membrane, as shown in Fig. 3 where three spots could be tracked as a function of time (see also Movies S1 and S2†). A reconstruction of the spot positions (Fig. 3(b)) shows that they are dragged in the direction of the outer flow near the channel mid-plane until they reach the downstream stagnation point. There, they are re-directed towards the regions close to the top and bottom walls, where they make their way upstream slowly. This returns them to the channel centre plane at the upstream stagnation point, where their recirculating motion repeats itself. The relative velocities of the forward and backward motion, compared with the velocity of the outer flow, are shown in Fig. 3(c). In the case presented here, the velocity of the outer flow ($U = 2088 \pm 93\ \mu\text{m s}^{-1}$) is larger than the spot velocities along the edge ($1040 \pm 22\ \mu\text{m s}^{-1}$) and it is many times faster than the backward velocity when the spots appear in the central region of the vesicle ($97 \pm 6\ \mu\text{m s}^{-1}$).

Such motion has attracted much attention due to its importance in biological and synthetic systems. Indeed, recirculating motion due to the outer fluid has already been reported in red blood cells or GUVs under different conditions: under shear flow far from a wall,^{32–35} close to a wall,^{36,37} and adhering to a wall.^{38–40} Physical models have also been developed to explain this behaviour and to relate it to the physical properties of the membrane. While the physical origin of the recirculation in the present case is the same as described before, our microfluidic approach allows for a long term observation of the motion on the interface without dewetting the GUV.

3. Shape of a trapped vesicle

Upon electro-formation GUVs are approximately spherical. When a GUV whose diameter is larger than the channel height flows into the microfluidic device, it must deform due to the geometric confinement, which increases the elastic energy of the membrane. Once inside the well, the GUV recovers its spherical shape when the flow is turned off, as long as its original diameter is smaller than the total height of the channel and the well, $60\ \mu\text{m}$. The corresponding reduction in the surface area creates an energy gradient and allows the vesicle to remain anchored against an external flow.

The transition in shape from the unconfined to the confined state can be observed by imposing a moderate flux of the outer fluid while imaging a trapped vesicle with confocal microscopy (Fig. 4). Here, three dimensional reconstructions of the shape of stationary vesicles are obtained from images in successive x - y

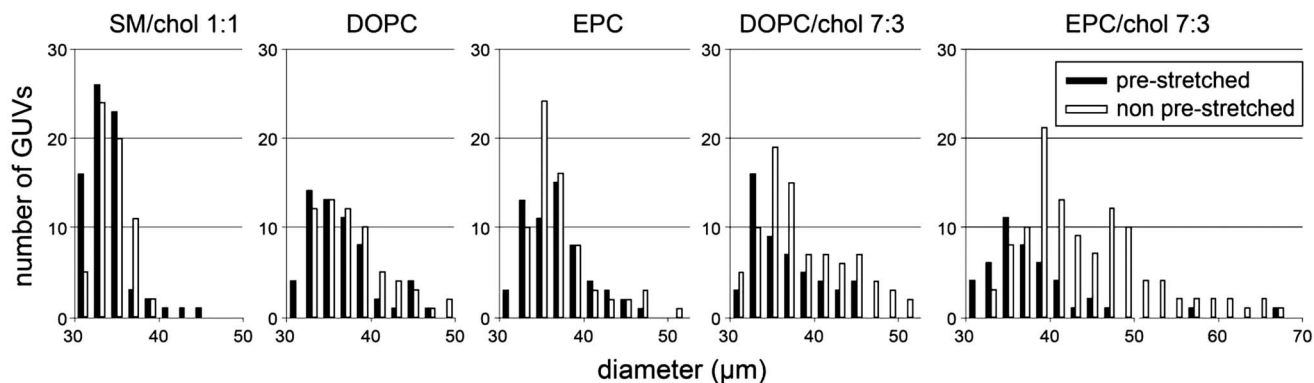


Fig. 2 Size distribution of trapped GUVs with different lipid compositions. Diameters were measured at zero flow. When GUVs are under hypo-osmotic conditions, *i.e.* 3 mM sucrose solution inside GUVs and water outside, the size distributions are narrower (pre-stretched GUVs, filled bars) compared to that under equi-osmotic conditions, *i.e.* with water both inside and outside of GUVs (non-pre-stretched GUVs, open bars). The ratios of the lipids are in mol/mol.

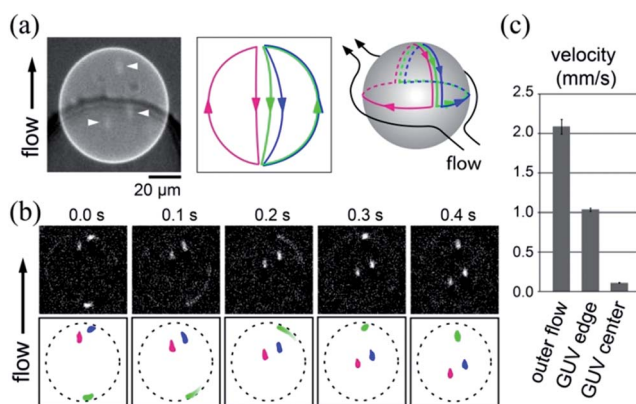


Fig. 3 Flow in the lipid bilayer membrane of a trapped GUV induced by outer medium flow observed from the bottom of the channel. (a) Left: fluorescence image of the trapped GUV with bright spots on its membrane together with the transmission image of the edge of a well (Movie S1†). The bright spots are indicated with arrow heads. Middle: trajectories of these spots obtained by superposition of 10 sequential images. Right: illustration of the three dimensional view. (b) The fluorescence signals of those bright spots are extracted by sequential image subtraction (Movie S2†). The upper panel shows a sequence of the subtracted images taken every 100 ms, depicted in the lower panel. The lipid flow velocity was measured with these images. (c) Velocities of outer medium flow, lipid flow at the edge of the GUV, and lipid flow crossing the center of the GUV. Error bars represent standard deviation.

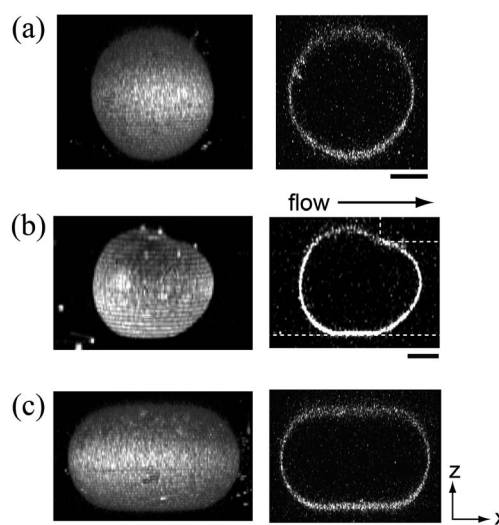


Fig. 4 Left, three dimensional reconstruction of confocal microscopy images of three different GUVs composed of 70% EPC and 30% cholesterol (mol/mol). (a) Trapped in a well without flow, (b) trapped in a well under a flow from left to right ($\Delta P = 50$ mbar), and (c) confined outside a well, without flow. Right, cross-sections of left images in an $x-z$ plane. In (b), the GUV is deformed at the edge of the well. The channel walls are indicated with dashed lines in the right panel. Bars, 10 μm .

planes stacked in the z direction (left), in addition to cross-sections of the three dimensional reconstruction in an $x-z$ plane (right). When the vesicle is in the well and in the absence of flow, it takes a spherical shape as shown in Fig. 4(a). When a moderate flow is imposed, the vesicle is pushed against the microchannel walls by the outer flow, causing the membrane to deform both at the corner of the anchor and on the bottom wall (Fig. 4(b)). Finally, the vesicle in the thin region of the microchannel is visualized in Fig. 4(c), and we observe that the top and bottom are flattened against the microchannel walls.

When the outer flow is increased beyond a critical value, U_c , the vesicle is released from the anchor, when the drag force on

the vesicle exceeds the aforementioned energy gradient (Movie S3†).

Three-dimensional images of this transition are not possible to acquire however, since the GUV begins to move quickly.

4. Critical flow velocity for untrapping GUVs depends on their size

As described in the Materials and methods section, we measured the initial radii, R_0 , of individually trapped, spherical GUVs in wells without flow. The critical flow velocities, U_c , corresponding to a critical pressure drop ΔP_c , to move these GUVs away from traps are plotted against R_0 in Fig. 5 for pre-

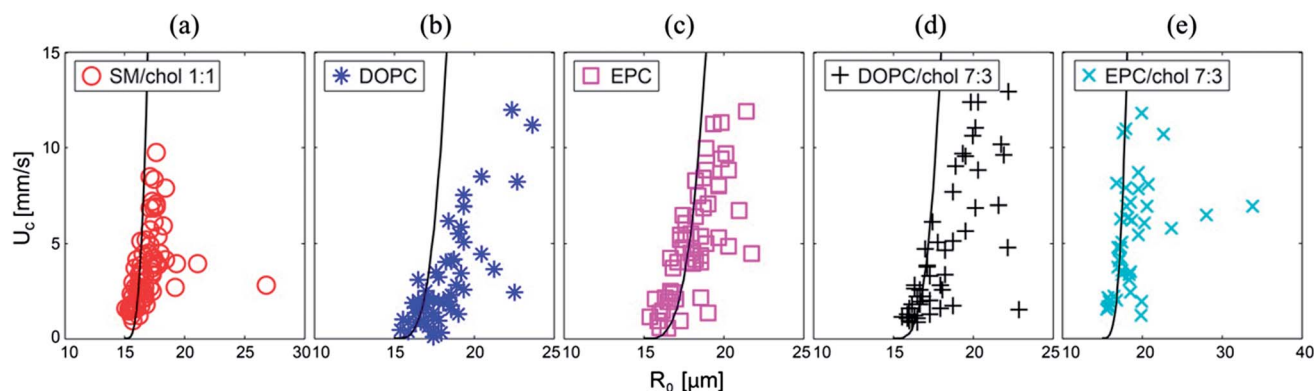


Fig. 5 Experimental measurements of the threshold flow velocity U_c for GUV untrapping versus the non-constrained GUV radius R_0 for (a) SM–chol 1 : 1, (b) DOPC, (c) EPC, (d) DOPC–chol 7 : 3, and (e) EPC–chol 7 : 3 (mol/mol). Solid lines correspond to the plot with eqn (6), and the stretching moduli given in Table 2.

stretched GUVs with different lipid compositions. These graphs show a clear dependence of U_c on R_0 .

In contrast with the data for pre-stretched GUVs, the relationship between size and critical velocity for non-pre-stretched GUVs shows a noisier distribution. More importantly, the values of U_c in the case of EPC–chol 7 : 3 GUVs are insensitive to R_0 (ESI Fig. S3†), which we attribute to the presence of surface defects in the lipid bilayer. Such defects are expected to exist in different proportions for all lipid compositions, and for different GUV preparation methods.⁴¹ Our data clearly illustrate that pre-stretching the GUVs helps in reducing the defects and is required for a proper mechanical characterization of lipid membranes. For this reason, we only treat the measurements obtained after pre-stretching in the following.

Model

In order to establish the mechanism underlying the trapping of the lipid GUV, we have developed a model in which the membrane is described as an elastic material that encloses a fixed volume of fluid. In addition, the GUV is either squeezed into a channel and highly stretched or trapped in the well and has low stretching. The prediction of the trapping force is then compared with an estimate of the drag force produced by the outer flow, which yields the critical velocity required to untrap it from the well.

1. Free energy of the vesicle membrane

The membrane of a vesicle can be modeled as a continuous two-dimensional surface that resists area dilation and bending.^{2,4} Thus, the free energy of the membrane, E , consists of surface stretching energy, E_s , and bending energy, E_b . The GUV bending energy corresponds to $E_b = \frac{k_c}{2} \int k^2 dA$, where k is the mean curvature of the vesicle surface and k_c is the bending rigidity. Our model does not include a Gaussian curvature term in E_b , since the membrane topology remains constant in our experiments.^{2–4} In the present problem, we estimate the magnitude of

Table 1 k_c values of different lipid compositions, from the literature

Lipid composition	k_c (10^{-20} J)
SM–chol 1 : 1	31 ± 2 (22 °C) ⁴⁴
DOPC	7.6 (30 °C) ⁴⁵
DOPC–chol 7 : 3	7.4 (30 °C) ⁴⁵
EPC	4.25 ± 0.87 (23–25 °C) ¹⁰
EPC–chol 7 : 3	14.4 ± 5.6 (22 °C) ⁴⁶

E_b to be $E_b = 8\pi k_c \approx 2 \times 10^{-18}$ J, based on the typical membrane bending rigidity $k_c \sim 10^{-19}$ J, as given in Table 1.

The stretching energy of a vesicle is $E_s = \sigma(A - A_0) = \sigma\Delta A$, where A_0 is the membrane area in the zero tension state. In contrast to drops and bubbles however, σ increases with surface deformation in two tension-dependent regimes.⁴ In the low-tension regime (for $\sigma < \sim 10^{-4}$ N m⁻¹), σ increases logarithmically with increasing ΔA , while in the high-tension regime, $\sigma = K_A \Delta A / A_0$. Here, the expansion parameter K_A is a material constant that depends on the lipid composition (Table 2).

For the analysis, we focus on pre-stretched vesicles only; they are tensed due to the hypo-osmotic conditions and thus are in the second regime. Although they are not in the zero-tension state, we assume that their spherical area is equivalent to A_0 . Then, assuming a 1% relative area stretching, E_s is estimated to be 3×10^{-14} J with a vesicle radius of 15 μm and $K_A \sim 100$ mN m⁻¹ (Table 2), which is nearly 4 orders of magnitude larger than

Table 2 K_A values of different lipid compositions, from the literature

Lipid composition	K_A (mN m ⁻¹)
SM–chol 1 : 1	2193 ± 209 (30 °C) ⁸
DOPC	310 ± 20 (15 °C) ⁸
DOPC–chol 7 : 3	420 (30–33 °C) ⁴⁵
EPC	167 ± 23 (14 °C) ⁴⁷
POPC ^a –chol 7 : 3	354 ± 5 (25 °C) ⁴⁸

^a Predominant component of EPC.

E_b . Therefore, we reasonably neglect the bending energy in calculating the vesicle shape.

We deduced A_0 and the volume of each GUV from its fluorescence image at zero flow, by measuring its diameter in the well (Fig. 4(a)). When the vesicle exits the well and becomes confined (Fig. 4(c)), it departs from a spherical configuration while keeping its volume. The new shape is determined by minimizing the change in surface energy from the spherical state,

$$\Delta E = K_A \frac{\Delta A^2}{A_0} \quad (1)$$

which is equivalent to minimizing A . Mathematically, minimal surfaces for a fixed volume have a constant mean curvature (e.g. a sphere if unconstrained), subject to boundary conditions. When the vesicle is confined by the channel height, the unconstrained part of the vesicle must have a constant mean curvature, which can be represented as axisymmetric surfaces called nodoids as illustrated in Fig. 6(a).⁴²

Following the formulation of ref. 43, the radial and vertical coordinates of the nodoid, $r(s)$ and $z(s)$, are given by the following parametric equations in terms of the independent variable, s :

$$r(s) = \frac{1}{c} \sqrt{1 + b^2 + 2b \sin cs}, \quad (2)$$

$$z(s) = \int_0^s \frac{1 + b \sin cu}{\sqrt{1 + b^2 + 2b \sin cu}} du, \quad (3)$$

where b and c are shape constants that determine the volume enclosed by the nodoid. For instance, the case of $b = 1$ and $c = 2$ corresponds to a spherical shape, as it is plotted in Fig. 6(b). Based on eqn (2) and (3), we numerically computed the nodoid

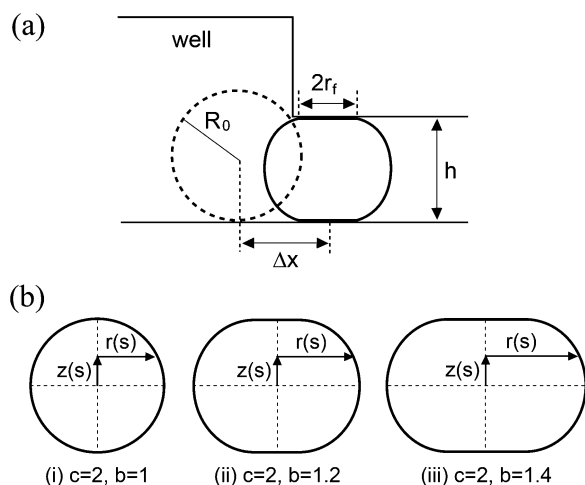


Fig. 6 (a) Schematic of the vesicle confined inside the microchannel. The vesicle shape (i.e. a nodoid) has a constant mean curvature where it is unconfined, which minimizes the change in free energy for a given vesicle volume. (b) Varying nodoid shapes plotted for $c = 2$ and for increasing values of b . $r(s)$ and $z(s)$ are radial and vertical coordinates of the nodoid. The parameter $b = 1$ corresponds to a sphere (i), while $b = 1.2$ (ii) and $b = 1.4$ (iii) lead to nodoidal curves of bigger volume that are flattened on the top and bottom surfaces.

shape, $r(s)$ and $z(s)$, for varying values of b and c , subject to the no-slope condition, $dz/dr = 0$, at $z = 0$ and $h = 30 \mu\text{m}$. Once $r(s)$ and $z(s)$ are known, the nodoid surface area, A , and the enclosed volume, V , are calculated *via* numerical integration in MATLAB. Finally, as the volume is constant, one can easily relate A to the radius, R_0 , and surface area, $A_0 = 4\pi R_0^2$, of the corresponding spherical vesicle based on $V = 4\pi R_0^3/3$. This yields $\Delta A/A_0$, which we plot at the bottom of Fig. 7.

2. Critical release velocity based on force balance

Once the shape of the confined vesicle is known, the gradient in surface energy is estimated as $\Delta E/\Delta x$, where Δx is the minimum distance that a spherical vesicle needs to travel in order to become untrapped, as illustrated in Fig. 6(a). This minimum distance depends on R_0 (top of Fig. 7) as

$$\Delta x = r_f + \sqrt{R_0^2 - \frac{h^2}{4}}, \quad (4)$$

where r_f is the base radius of the squeezed vesicle. Eqn (1) and (4) can then be combined to yield the trapping force

$$F_{\text{trap}} = K_A \frac{\Delta A^2}{A_0 \Delta x}. \quad (5)$$

This force must balance the viscous drag force that we estimate as $F_{\text{drag}} = 6\pi\mu UR_0$, where μ is the viscosity of water and U is the external flow velocity. Note that the prefactor of the drag force might be slightly higher due to the geometry⁴⁹ but has not been exactly calculated for our experimental conditions. Then, a critical value of the drag force occurs when U reaches a critical value U_c .

Based on a force balance between the drag force and the gradient of surface energy (i.e., $F_{\text{drag}} = F_{\text{trap}}$), the critical velocity, U_c , is computed as

$$U_c = \frac{K_A \Delta A^2}{6\pi\mu \Delta x A_0 R_0}. \quad (6)$$

The evolution of U_c from eqn (6) is plotted in Fig. 8, using the stretching moduli given in Table 2, along with the data for

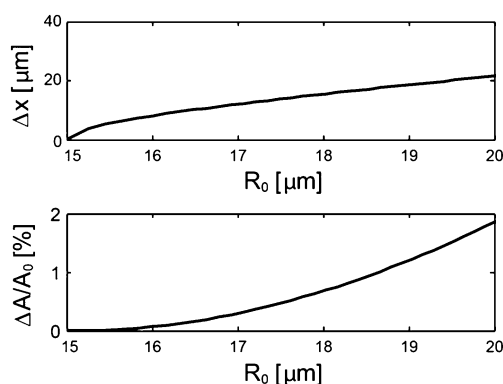


Fig. 7 Plots of Δx versus vesicle radius, R_0 (top) and of membrane deformation, $\Delta A/A_0$ versus R_0 (bottom).

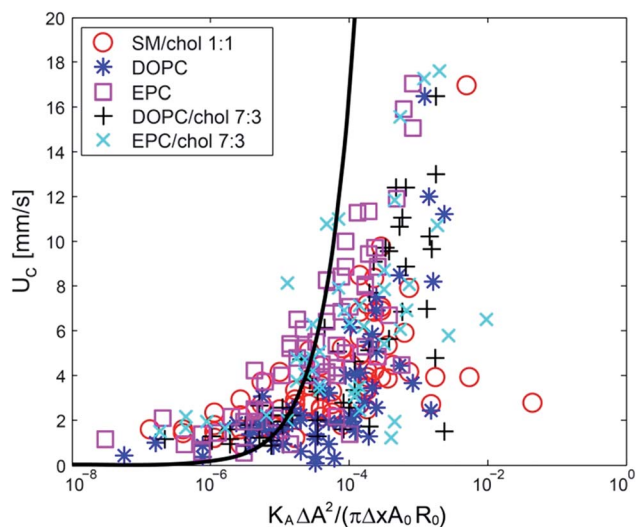


Fig. 8 Plot of experimental critical velocity U_c versus $K_A \Delta A^2 / (\pi \Delta x A_0 R_0)$ (log scale) for pre-stretched vesicles and different lipid compositions. The solid line is the plot of the theoretical prediction (eqn (5)) using the stretching moduli from the literature (Table 2), which matches well the experimental data for small deformations, ΔA .

pre-stretched vesicles. The radius of the unconfined vesicle, R_0 , was measured experimentally, which yields the initial surface area, $A_0 = 4\pi R_0^2$, and the corresponding vesicle volume, $V = 4\pi R_0^3/3$. Then, we numerically computed the increase in surface area, $\Delta A = A - A_0$, when the vesicle enters the channel of height $h = 30 \mu\text{m}$, by assuming a nodoidal shape (described by eqn (2) and (3), as previously discussed) and for constant volume. In addition, the characteristic release distance, Δx , was easily calculated with the known vesicle shape, based on eqn (4). We find good agreement between the model prediction and the experiments, particularly for small deformations, as evident in Fig. 5 and 8.

Discussion and conclusion

In this work, we show that GUVs can be trapped inside wells etched on the surface of a microfluidic device due to the relaxation of the membrane stretching energy. The force balance between the drag force and the force due to the increase of surface energy of the GUVs yields a general form that recalls the force balance for liquid droplets. Several important differences appear nevertheless, due to the nature of the vesicle membrane and the differences in the geometry of the anchors. Most importantly, the relative inextensibility of the GUV membrane implies that only vesicles whose diameter is close to the channel height can be trapped by this system of anchors. Indeed, the values of $\Delta A/A_0$ that we are able to reach are limited to a few percent. This is consistent with previous observations that vesicles will rupture if their surface area is increased beyond around 5%. Nonetheless, this elastic energy change is sufficient to allow the trapping of the vesicles in the microfluidic devices.

In contrast with previous studies on the trapping of droplets or air bubbles in microfluidic anchors,^{26–28} the wells here are larger than the object that is being trapped. As a result, the characteristic distance over which the surface energy changes depends on the radius of the trapped object rather than on the well diameter (Fig. 6(a)). The resulting trapping force therefore has a complex dependence on the GUV radius. Indeed, we find that larger GUVs are more difficult to extract from the anchors than smaller GUVs, as seen by the higher value of the critical velocity U_c for large vesicles. This behaviour is universal for all of the lipids tested here, as shown in Fig. 5. It contrasts strongly with the behaviour of droplets in small anchors, where larger droplets require a smaller flow velocity to extract them.²⁷

In practical terms, this method contrasts with the traditional micropipette aspiration method where only one GUV at a time can be studied by a trained experimentalist. The current device allows the measurement to be performed on typically 50 GUVs in a single experiment but this number can be increased to several thousands by modifying the number of traps. The size selectivity can provide an interesting advantage by ensuring that the parallel traps all contain GUVs of similar sizes. The actual sizes of the trapped GUV can easily be modified by changing the microchannel height. The theoretical model that is developed above provides predictions for the device behaviour as a function of the physical and geometric parameters. Moreover, our trapping method should apply to any GUV preparation (spontaneous formation, inverse emulsion-based method, jetting) (see ref. 6 for a review on methods), but the presence of defects or impurities in the membrane may affect the untrapping conditions.

Finally, this platform offers the possibility to flow successively several solutions around the anchored GUVs, for example, in order to bring proteins, nucleotides (ATP, GTP), or antibodies, as long as the flow velocity remains lower than the untrapping velocity for the GUVs. Such sequential binding experiments are currently very challenging with GUVs as they cannot be easily bound to substrates and they cannot sustain multiple centrifugations. With the rapid development of synthetic biology based on lipid systems,⁵⁰ developing such high-throughput methods may become particularly attractive.

Acknowledgements

We thank Caroline Frot for the microfabrication and Sophie Aimon for her help for the confocal microscopy observation. We thank Jean-Louis Viovy and Laurent Malaquin for providing their platform and for technical advices. We thank François Quemeneur and Alexandre Mamane for fruitful discussions. We thank the BioImaging Cell and Tissue Core Facility of the Institut Curie (PICK-IBISA) for technical support. A.Y. was supported by the Agence Nationale pour la Recherche (grant ANR-09-0027-03). P.B.'s group belongs to the CNRS consortium CellTiss. CNB thanks Institut Curie for its hospitality during a sabbatical period that initiated this project. Part of this work was funded by the European Research Council (ERC) through the Starting Grant Agreement 278248 "Multicell".

Notes and references

- 1 M. Bloom, E. Evans and O. G. Mouritsen, *Q. Rev. Biophys.*, 1991, **24**, 293–397.
- 2 W. Helfrich, *Z. Naturforsch., C: Biochem., Biophys., Biol., Virol.*, 1973, **28**, 693–703.
- 3 P. B. Canham, *J. Theor. Biol.*, 1970, **26**, 61–81.
- 4 E. Evans and W. Rawicz, *Phys. Rev. Lett.*, 1990, **64**, 2094.
- 5 P. Sens, L. Johannes and P. Bassereau, *Curr. Opin. Cell Biol.*, 2008, **20**, 476–482.
- 6 P. Walde, K. Cosentino, H. Engel and P. Stano, *ChemBioChem*, 2010, **11**, 848–865.
- 7 W. Rawicz, K. C. Olbrich, T. McIntosh, D. Needham and E. Evans, *Biophys. J.*, 2000, **79**, 328–339.
- 8 W. Rawicz, B. A. Smith, T. J. McIntosh, S. A. Simon and E. Evans, *Biophys. J.*, 2008, **94**, 4725–4736.
- 9 P. Meleard, T. Pott, H. Bouvrais and J. H. Ipsen, *Eur. Phys. J. E: Soft Matter Biol. Phys.*, 2011, **34**, 116.
- 10 J. Pécéréaux, H. G. Dobreiner, J. Prost, J. F. Joanny and P. Bassereau, *Eur. Phys. J. E: Soft Matter Biol. Phys.*, 2004, **13**, 277–290.
- 11 A. A. Bhagat, H. Bow, H. W. Hou, S. J. Tan, J. Han and C. T. Lim, *Med. Biol. Eng. Comput.*, 2010, **48**, 999–1014.
- 12 J. P. Frimat, M. Becker, Y. Y. Chiang, U. Marggraf, D. Janasek, J. G. Hengstler, J. Franzke and J. West, *Lab Chip*, 2011, **11**, 231–237.
- 13 C. H. Schmitz, A. C. Rowat, S. Koster and D. A. Weitz, *Lab Chip*, 2009, **9**, 44–49.
- 14 W.-H. Tan and S. Takeuchi, *Proc. Natl. Acad. Sci. U. S. A.*, 2006, **104**, 1146–1151.
- 15 T. Teshima, H. Ishihara, K. Iwai, A. Adachi and S. Takeuchi, *Lab Chip*, 2010, **10**, 2443–2448.
- 16 G. G. H. Noguchi, L. Schmid, A. Wixforth and T. Franke, *Europhys. Lett.*, 2010, **89**, 29002.
- 17 G. Coupier, A. Farutin, C. Minetti, T. Podgorski and C. Misbah, *Phys. Rev. Lett.*, 2012, **108**, 178106.
- 18 M. Abkarian, M. Faivre and H. A. Stone, *Proc. Natl. Acad. Sci. U. S. A.*, 2006, **103**, 538–542.
- 19 M. Abkarian, M. Faivre, R. Horton, K. Smistrup, C. A. Best-Popescu and H. A. Stone, *Biomed. Mater.*, 2008, **3**, 034011.
- 20 P. Preira, M.-P. Valignat, J. Bico and O. Théodoly, *Biomicrofluidics*, 2013, **7**, 024111.
- 21 F. Risso, F. Collé-Paillot and M. Zagzoule, *J. Fluid Mech.*, 2006, **547**, 149–173.
- 22 Y. Lefebvre, E. Leclerc, D. Barthès-Biesel, J. Walter and F. Edwards-Lévy, *Phys. Fluids*, 2008, **20**, 123102.
- 23 J. T. Cabral and S. D. Hudson, *Lab Chip*, 2006, **6**, 427–436.
- 24 A. Huebner, D. Bratton, G. Whyte, M. Yang, A. J. Demello, C. Abell and F. Hollfelder, *Lab Chip*, 2009, **9**, 692–698.
- 25 J. U. Shim, G. Cristobal, D. R. Link, T. Thorsen, Y. Jia, K. Piattelli and S. Fraden, *J. Am. Chem. Soc.*, 2007, **129**, 8825–8835.
- 26 P. Abbyad, R. Dangla, A. Alexandrou and C. N. Baroud, *Lab Chip*, 2011, **11**, 813–821.
- 27 R. Dangla, S. Lee and C. N. Baroud, *Phys. Rev. Lett.*, 2011, **107**, 124501.
- 28 S. Lee, F. Gallaire and C. N. Baroud, *Soft Matter*, 2012, **8**, 10750–10758.
- 29 P. P. K. Stephan, L. Renaud, P. Kleimann, P. Morin, N. Ouaini and R. Ferrigno, *J. Micromech. Microeng.*, 2007, **17**, N69–N74.
- 30 L. Mathivet, S. Cribier and P. F. Devaux, *Biophys. J.*, 1996, **70**, 1112–1121.
- 31 K. Olbrich, W. Rawicz, D. Needham and E. Evans, *Biophys. J.*, 2000, **79**, 321–327.
- 32 V. Kantsler and V. Steinberg, *Phys. Rev. Lett.*, 2005, **95**, 258101.
- 33 M. Abkarian, M. Faivre and A. Viallat, *Phys. Rev. Lett.*, 2007, **98**, 188302.
- 34 J. M. Skotheim and T. W. Secomb, *Phys. Rev. Lett.*, 2007, **98**, 078301.
- 35 S. Messlinger, B. Schmidt, H. Noguchi and G. Gompper, *Phys. Rev. E: Stat., Nonlinear, Soft Matter Phys.*, 2009, **80**, 011901.
- 36 M. Abkarian, C. Lartigue and A. Viallat, *Phys. Rev. Lett.*, 2002, **88**, 068103.
- 37 M. Abkarian and A. Viallat, *Biophys. J.*, 2005, **89**, 1055–1066.
- 38 B. Lorz, R. Simson, J. Nardi and E. Sackmann, *Europhys. Lett.*, 2000, **51**, 468–474.
- 39 C. Vézy, G. Massiera and A. Viallat, *Soft Matter*, 2007, **3**, 844–851.
- 40 A. R. Honerkamp-Smith, F. G. Woodhouse, V. Kantsler and R. E. Goldstein, *Phys. Rev. Lett.*, 2013, **111**, 038103.
- 41 N. Rodriguez, F. Pincet and S. Cribier, *Colloids Surf., B*, 2005, **42**, 125–130.
- 42 J. F. Opera, *Differential Geometry and its Applications*, Mathematical Association of America, 2007.
- 43 M. A. Verges, M. C. Larson and R. Bacou, *Exp. Mech.*, 2001, **41**, 351–357.
- 44 A. Roux, D. Cuvelier, P. Nassoy, J. Prost, P. Bassereau and B. Goud, *EMBO J.*, 2005, **24**, 1537–1545.
- 45 J. Pan, S. Tristram-Nagle and J. F. Nagle, *Phys. Rev. E: Stat., Nonlinear, Soft Matter Phys.*, 2009, **80**, 021931.
- 46 X. Liang, G. Mao and K. Y. Ng, *J. Colloid Interface Sci.*, 2004, **278**, 53–62.
- 47 T. J. McIntosh, S. Advani, R. E. Burton, D. V. Zhelev, D. Needham and S. A. Simon, *Biochemistry*, 1995, **34**, 8520–8532.
- 48 J. Henriksen, A. C. Rowat, E. Brief, Y. W. Hsueh, J. L. Thewalt, M. J. Zuckermann and J. H. Ipsen, *Biophys. J.*, 2006, **90**, 1639–1649.
- 49 H. J. Keh and P. Y. Chen, *Chem. Eng. Sci.*, 2001, **56**, 6863–6871.
- 50 P. Schuille, *Science*, 2011, **333**, 1252–1254.